



Effect of mechanical activation on the structure and ferroelectric property of $\text{Na}_{0.5}\text{K}_{0.5}\text{NbO}_3$

Laijun Liu^{a,b,c,*}, Meixia Wu^a, Yanmin Huang^a, Liang Fang^a, Huiqing Fan^b,
Hichem Dammak^c, Mai Pham Thi^d

^aKey Laboratory of Nonferrous Materials and New Processing Technology, Ministry of Education, Guilin University of Technology, Guilin 541004, China

^bState Key Laboratory of Solidification Processing, School of Materials Science and Engineering, Northwestern Polytechnical University, Xi'an 710072, China

^cLaboratoire Structures, Propriétés et Modélisation des Solides, Ecole Centrale Paris, CNRS-UMR8580, Grande voie des Vignes, 92295 Châtenay-Malabry Cedex, France

^dTHALES Research & Technology France, Campus Polytechnique, 1 Avenue Augustin Fresne, 91767 Palaiseau Cedex, France

ARTICLE INFO

Article history:

Received 4 December 2010

Received in revised form 8 April 2011

Accepted 3 May 2011

Available online 7 May 2011

Keywords:

A. Ceramics
D. Crystal structure
D. Defects
D. Ferroelectricity

ABSTRACT

Mechanical activation synthesis of $\text{Na}_{0.5}\text{K}_{0.5}\text{NbO}_3$ (NKN) was studied in order to explore the effect of mechanochemical interaction on the crystal structure and microstructure of NKN powder and ceramic. A single phase, nanocrystalline perovskite NKN powder has been derived from a mixture of oxide/carbonates via a mechanical activation route with heating at an elevated temperature. With the increase in milling time, the distortion of orthorhombic structure for NKN was weakened and the cell volume of NKN powder slightly decreased. The relative density and remnant polarization of NKN ceramics were improved, and the grain became uniform and smaller for prolonged milling NKN. The developed method is well suited for the production of NKN nanocrystallite powders and refined grain NKN ceramics.

© 2011 Elsevier Ltd. All rights reserved.

1. Introduction

$\text{Na}_{0.5}\text{K}_{0.5}\text{NbO}_3$ (NKN) is a well known lead-free piezoelectric material with suitable characteristics for applications as piezoelectric devices due to the combination of a high electromechanical coupling coefficient ($k_p > 30\%$) and low dielectric constant ($\epsilon < 500$) [1,2]. However, it is difficult to fabricate well-sintered NKN ceramics in air atmospheric [3], and the density of NKN was enhanced by using the hot-pressing technique [4,5] and sintering aids [6,7]. One of the reasons for the poor sinterability of NKN ceramics is the low melting point of KNbO_3 compared with other ferroelectric materials. Furthermore, sodium and potassium ions of NKN ceramics easily evaporated at high temperature. Particle coarsening often takes place during traditional synthesis, which in turn diminishes the sinterability of the resulting powder and deteriorates the piezoelectric response. Consequently, reduction in initial particle size is often considered due to the fact that the driving force for sintering is inversely proportional to the size of particle. One of the ways to minimize grain size and avoid Na/K evaporation is mechanical activation method.

The intrinsic advantage of mechanical alloying is its ability to enhance a solid state reaction through mechanical activation, instead of calcining at a high temperature. Mechanical alloying was initially used for the production of intermetallic and alloy compounds [8]. It can also lead to an improvement in the reactivity of starting materials and therefore the desired ceramics phase is formed at a low calcination temperature [9,10]. In the last few years, great efforts have been made in order to synthesize various ceramic compounds by mechanical activation method starting from a powder mixture of carbonates or oxides [11–14].

In order to understand the relationship between preparation conditions and the synthesis process and microstructure of NKN, $\text{Na}_2\text{CO}_3\text{--K}_2\text{CO}_3\text{--Nb}_2\text{O}_5$ mixture was processed by mechanical activation method for different triggering times. Additionally, the influence of milling time on the distortion of orthorhombic lattice and the change of cell volume of NKN was also considered.

2. Experimental

The raw materials used in this study were sodium carbonate (Na_2CO_3 , PROLABO, 99.9%, $d_{50} \sim 9 \mu\text{m}$), potassium carbonate (K_2CO_3 , MERCK, 99.995%, average particle size $d_{50} \sim 13 \mu\text{m}$), and niobium oxide (Nb_2O_5 , 99.5%, INTERCHIM, $d_{50} \sim 2 \mu\text{m}$). In all the experiments, the raw materials were dried right before use at 200°C for 12 h because of their hygroscopic nature. The high-energy ball-milling was carried out in a planetary mill Retsch PM

* Corresponding author at: Key Laboratory of Nonferrous Materials and New Processing Technology, Ministry of Education, Guilin University of Technology, Guilin 541004, China. Tel.: +86 7735893395; fax: +86 7735896290.

E-mail address: ljliu2@163.com (L. Liu).

100 with tungsten carbide (WC)–Co milling tools, specially equipped for mechanical alloying, operating the rotational speed of 450 rpm. The mixtures of the starting compounds were weighed and placed in the vial with a ball-to-powder weight ratio of 25:1. The powders were mechanical alloying treated for various times ranging from 1 to 20 h. After calcined at 850 °C for 2.5 h to obtain pure NKN powder, the resulting powder was uniaxially pressed into discs of 10 mm in diameter and 2 mm in thickness under 300 MPa and then pressed under 650 MPa with cool isostatic pressing method. These discs were sintered at 1070 °C for 2 h in a sealed alumina crucible in air.

High resolution X-ray diffraction measurements were performed on a highly accurate two-axis diffractometer in a Bragg-Brentano geometry with $\text{Cu-K}\alpha$ and $\text{Cu-K}\beta$ wavelength issued from an 18 kW rotating anode generator with diffraction angle precision better than 0.002° (2θ). Selected regions of the diffractogram, containing the $\{0\ 0\ 2\}$, $\{0\ 2\ 2\}$, and $\{2\ 2\ 2\}$ pseudocubic reflections, were recorded. Because of complicated peak shapes, a very careful peak-fitting analysis was realized using TOPAS software to find the position of peaks. The average particle size (z -average size) was measured by photon correlation spectroscopy (PCS, Nano ZS90 zetasizer, Malvern Instruments Corp, UK) at 25 °C under a fixed angle of 90° in disposable polystyrene cuvettes. The measurements were obtained using a He–Ne laser of 633 nm. No multi-scattering phenomenon was observed. Measurements were performed in distilled water. The particle size and morphology of the thermally treated powders were evaluated using Transmission Electron Microscopy (TEM, HitachiH-7100 175) with an accelerating voltage of 120 kV. For TEM investigations, powders were suspended in isopropanol, and a drop of this suspension was deposited on a holey carbon-coated film supported on a 400-mesh copper grid. The microstructure of as-sintered samples was observed by a scanning electron microscope (SEM, JSM-6460LV, JEOL, Japan). To observe grain size and grain boundary by SEM, the sintered samples were polished and thermally etched. The P – E hysteresis loop was measured at 50 Hz at room temperature using a ferroelectric tester (TF Analyzer 2000, axiACCT, Germany). A poling treatment was conducted using a dc power supply at 2.0 kV/mm in silicon oil at room temperature for 30 min.

3. Results and discussion

Fig. 1 shows the XRD trace of the starting powder mixture consisting of Na_2CO_3 , K_2CO_3 and Nb_2O_5 of stoichiometric NKN composition, together with those subjected to 2, 6, 10, 14 and 20 h of mechanical activation, respectively. As expected, prior to mechani-

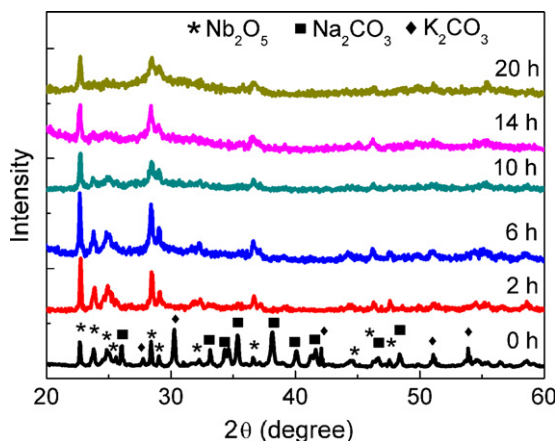


Fig. 1. XRD patterns of the oxide mixture of NKN composition subjected to 0, 2, 6, 10, 14 and 20 h of mechanical activation, respectively.

cal activation the powder mixture exhibits sharp peaks of crystalline Na_2CO_3 , K_2CO_3 and Nb_2O_5 , as no or little reaction was triggered by the manual mix. However, upon 2 h of mechanical activation, almost all the sharp peaks of mixed oxides have vanished except of Nb_2O_5 peaks. Furthermore, Nb_2O_5 peaks are still present after 10 h of milling and no new peak is formed. Further milling from 10 to 20 h does not influence the phase composition, showing that the mechanochemical reaction between Na_2CO_3 , K_2CO_3 and Nb_2O_5 , which would yield NKN, does not occur. After 20 h of milling the Nb_2O_5 peaks weaken, this may indicate that Nb_2O_5 is probably in an amorphous state. According to XRD, no formation of NaNbO_3 , KNbO_3 and NKN is observed even after 20 h of milling. Our results are different from Rojac's [15]. The difference may be attributed to milling speed and milling time. Based on Ref. [16], the ball-impact energy in our experiment is much more than 165 mJ/hit while Rojac's ball-impact energy is 35 mJ/hit.

In order to obtain pure NKN powder, the milled starting materials were calcined at 850 °C for 2.5 h. Fig. 2 shows the XRD patterns of calcined mixture with different mechanical activation times. All of compositions crystallized in a pure NKN perovskite phase (ICSD 0038004). No trace of the NaNbO_3 and KNbO_3 can be found in the patterns. Although the structure of NKN at room temperature is orthorhombic, the perovskite type ABO_3 subcell possesses monoclinic symmetry, with lattice parameters $a' = c' > b'$ while b' axis is perpendicular to $a'c'$ plane and angle β a little more than 90° . All the reflections could be indexed with monoclinic unit cell. No superlattice reflections were found in previous XRD measurements [17], so no cornerlinked O octahedra tilting should be taken into account [18].

$\{0\ 0\ 2\}$ and $\{0\ 2\ 2\}$ pseudocubic reflections of NKN compositions for different mechanical activation times are recorded in Fig. 3a and b, respectively. The positions of $(0\ 0\ 2)$ and $(0\ 2\ 0)$ peaks shift to high angle with the increase of mechanical activation time. The data of NKN milled 2 h, 4 h, 6 h and 18 h are slightly fluctuant, which could be caused by profile fitting errors. In Fig. 3b, it is very difficult to separate $(2\ 0\ 2)$ peak from $(2\ 2\ 0)$ and $(2\ 0\ 2)$ peaks when the mechanical activation time is less than 8 h. However, all of the peaks shift to high angle with the increase of mechanical activation time. It is suggested that the interplanar distance or cell volume of NKN crystal cell have changed with the increase of mechanical activation time.

Generally, there are two competing processes taking place during mechanical activation [19]. One is the wear debris from the WC milling tools. The amount of W, C and Co stem from the wear debris of the WC–Co milling tools will increase with increasing milling time. The other is grain refinement. Here we show the

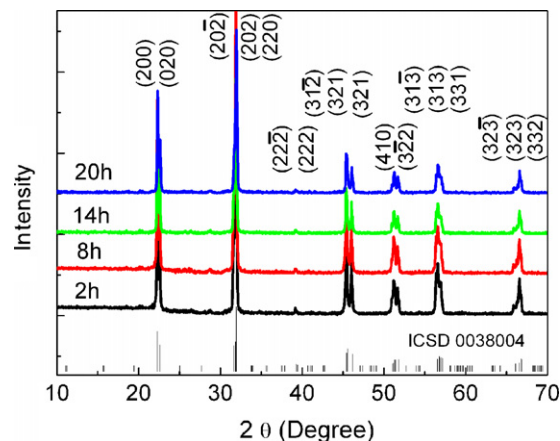


Fig. 2. XRD patterns of NKN nanocrystalline powder derived from the powder mechanically activated for different times and calcined at 850 °C for 2.5 h.

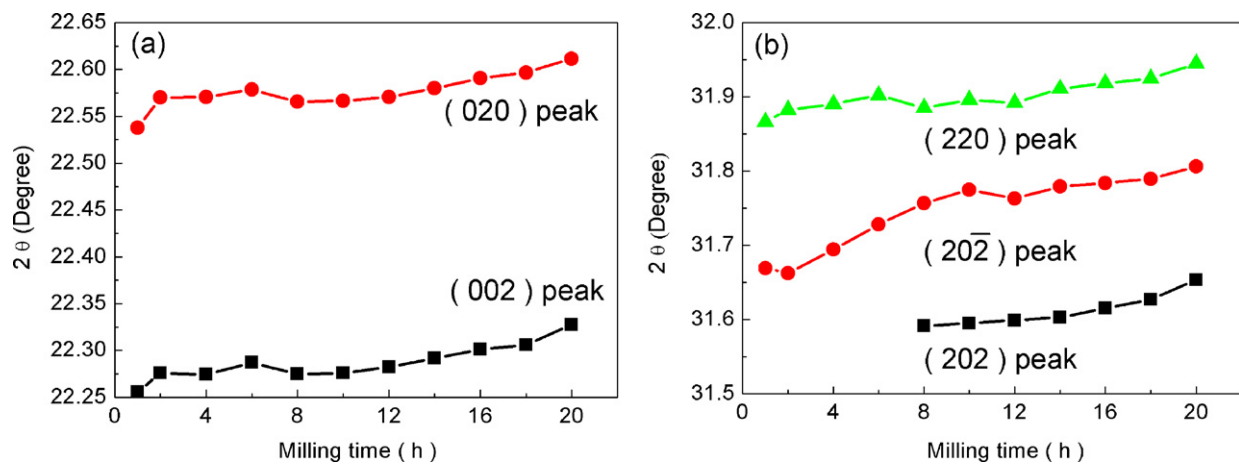


Fig. 3. Mechanical activation time dependence of the XRD peak positions of NKN nanocrystalline powder: (a) {002} peak; (b) {022} peak.

mechanical activation time dependence of average crystallite size of NKN in Fig. 4a. The average crystallite size was calculated from the full width at half maximum (FWHM) of the diffraction lines by using Topas 2P software according to Scherrer's relation:

$$d = \frac{K\lambda}{B \cos \theta} \quad (1)$$

where d is crystallite diameter, λ is X-ray wavelength, θ the diffraction angle, B is FWHM of the diffraction peak, and K is Scherrer constant (0.94 in our work). Here it should be pointed out that the FWHM has subtracted out the instrumental contribution to broadening and NKN powder was annealed in order to eliminate stress effect. At the beginning, the average crystallite size of NKN does not present obvious change with the increase of mechanical activation time. However, a slight decrease can be found when the mechanical activation time is more than 10 h. It may be caused by introduced impurity during mechanical activation since the introduced impurity induces point defects in NKN lattice and changes the atomic diffusion or gain growth of NKN during calcination.

The mean particle size and size distribution of NKN powder for milling 2 h and 20 h were also analyzed using the Zetasizer analysis, which are given in Fig. 4b and c, respectively. The mean particle sizes of NKN for milling 2 h and 20 h are 179.6 nm and 160.8 nm, respectively. Distribution profiles were fitted by Lorentz formulation, and obtained the particle sizes of NKN for milling 2 h and 20 h are 182.9 nm and 162.7 nm, respectively. Obviously, the mean particle size obtained by Zetasizer analysis is much larger than that of by Scherrer's relation; the difference may be consequent on agglomerate of NKN particle. Fig. 4d and e shows bright field TEM micrographs of the NKN powder triggered for 2 h and 20 h, respectively. They show particles with mean diameters of ~ 270 nm and ~ 190 nm in size for triggered 2 h and 20 h, respectively, but many of the individual primary particles were clustered into agglomerates. They are in good agreement with the tendency observed by Zetasizer analysis. It indicates that the observed nanoparticles are composed of crystalline material, forming polycrystalline particles since the calculated crystallite sizes are considerably smaller than the observed particle sizes.

Table 1 gives the cell parameters, cell volumes and c/a ratio of nanocrystalline NKN powder with different mechanical activation times. Cell parameters were refined using Fullprof software, which performs a full-pattern matching using the Rietveld method. A shift correction was made in order to obtain the correct zero position. The background was modeled using the Legendre polynomial and the peaks' profiles were refined using a pseudo-Voigt function. The chosen space group for these refinements for

orthorhombic phase was $Amm2$. The relationship between monoclinic and orthorhombic unit cells is given:

$$a = a' \sin\left(\frac{\beta}{2}\right) + c' \sin\left(\frac{\beta}{2}\right) \quad (2)$$

$$b = 2 \times b' \quad (3)$$

$$c = c' \cos\left(\frac{\beta}{2}\right) + a' \cos\left(\frac{\beta}{2}\right) \quad (4)$$

where a, b, c are the parameters of orthorhombic unit cell and a', b' and c' are the parameters of monoclinic unit cell. Cell parameters b and c , cell volume and c/a ratio decreased regularly with the increase of mechanical activation time, and thus to a more symmetrical orthorhombic unit cell.

The amount of WC is more than 95 wt% in our milling tools. Generally, hexavalent tungsten ion will substitute to quinquivalence niobium ion in NKN lattice. So introduced tungsten ion acts as a donor in NKN composition, which will lead to the increase of sodium/potassium vacancy. The ionic radius of quinquivalence niobium is 0.64 Å, and the ionic radius of hexavalent tungsten is 0.60 Å. Furthermore, the more tungsten is introduced, the higher concentration of sodium/potassium vacancies appears in NKN lattice. Therefore, the distortion of orthorhombic structure for NKN was weakened and the cell volume of NKN slightly decreased with the increase of mechanical activation time.

SEM photographs for polished and thermally etched NKN ceramics with different mechanical activation times are shown in Fig. 5. All of microstructure morphologies present non-compacted and bimodal distribution of grain size. The number of bigger grains ($\sim 8 \mu\text{m}$) and porosity decrease quickly with the increase of mechanical activation time. The change of relative density in Table 1 also can give similar results.

The driving force of grain growth can be increased by the creation of vacancies [20]. So a change in the vacancy concentration can affect the grain growth behavior. However, in experiments carried out on BaTiO_3 and SrTiO_3 , increasing the vacancy concentration (by ions doping or sintering in reducing atmospheres) caused a decrease of driving force. This will cause the grain growth behavior to change from abnormal to normal [21–23]. Since tungsten is introduced into NKN lattice during mechanical activation, cation vacancies such as sodium vacancy and potassium vacancy will induce in NKN lattice. The observed interface structure of grain, faceted or rough, depends on the dopant concentration, the concentration of cation vacancies linearly increases with the amount of added donor in an oxidizing atmosphere [21].

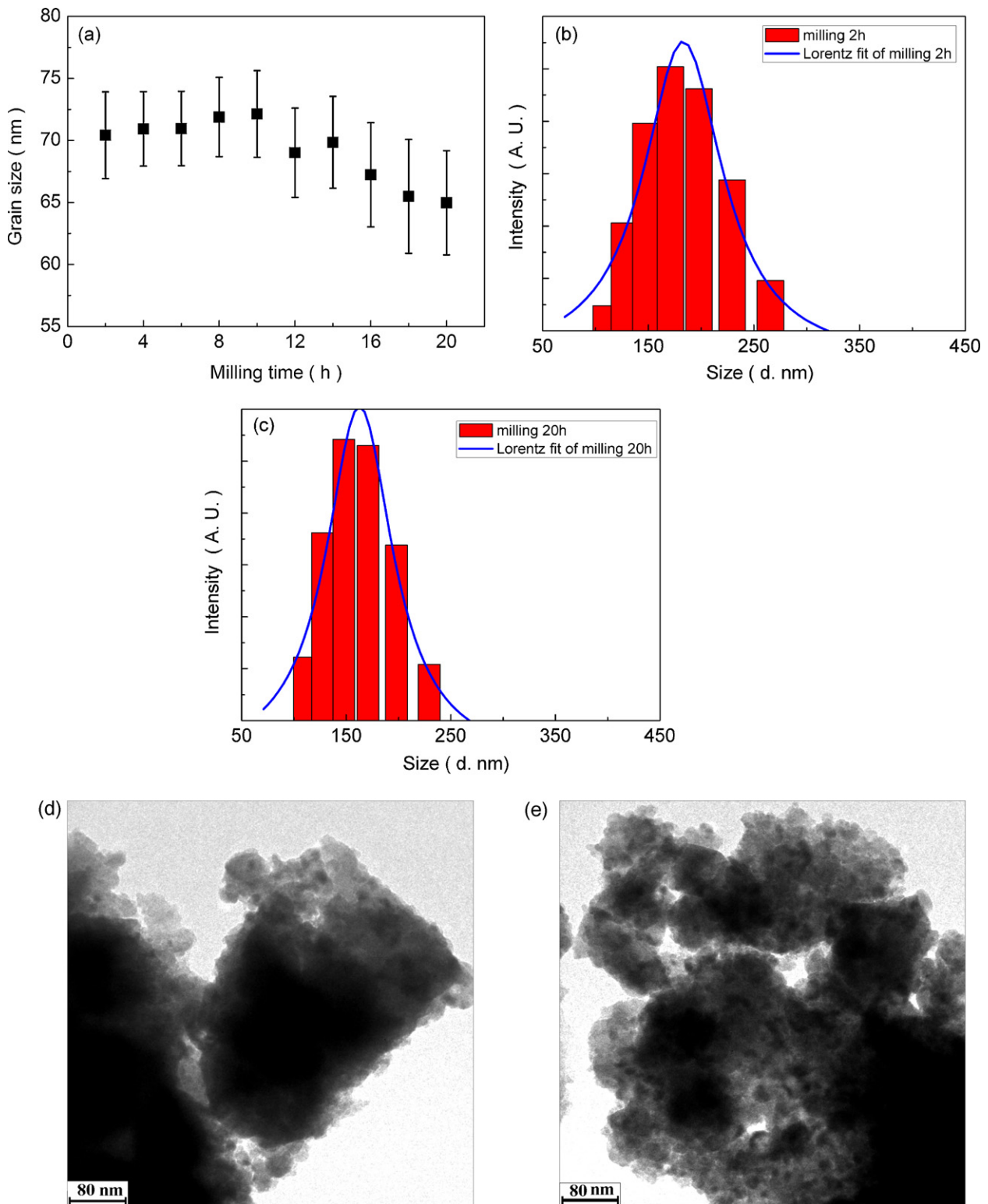


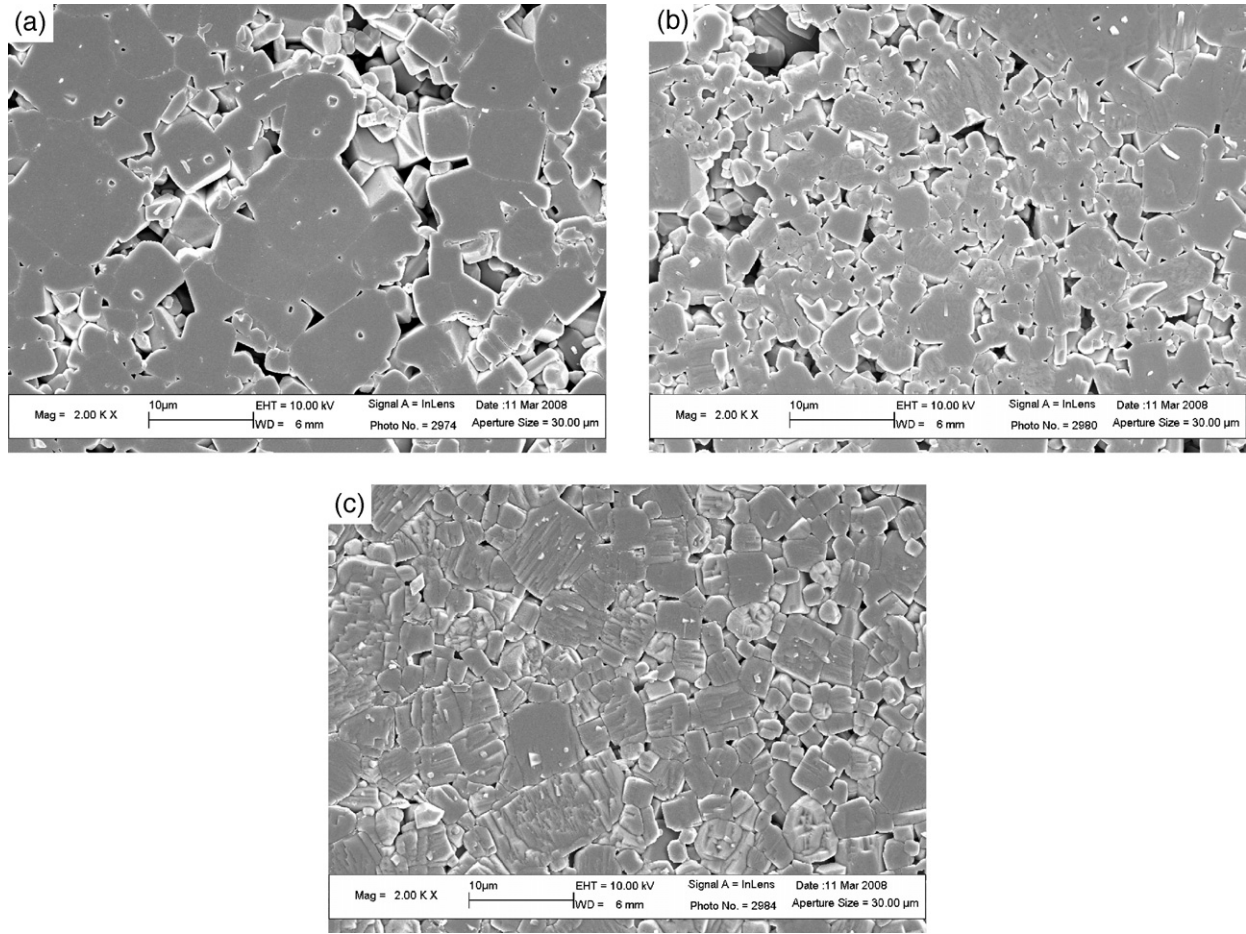
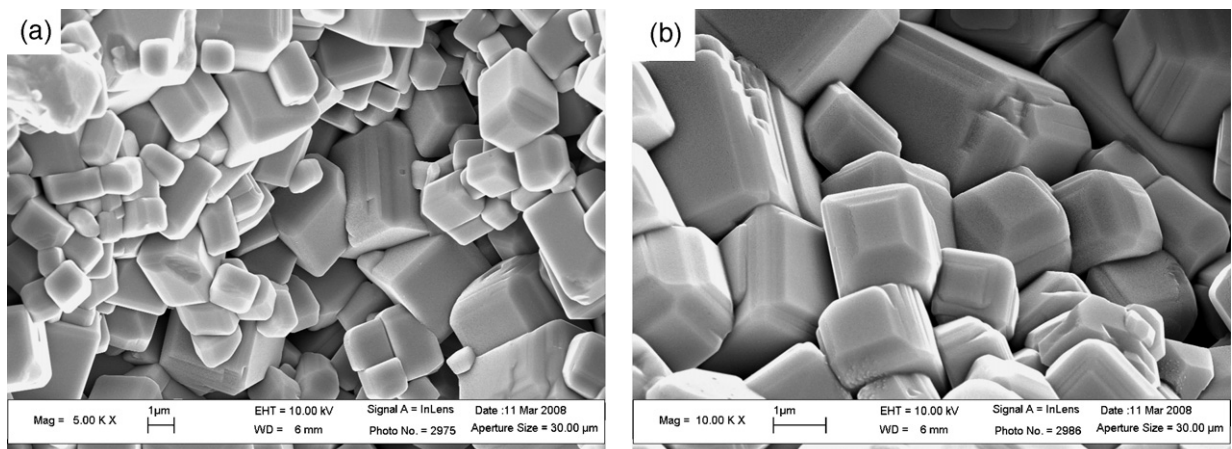
Fig. 4. (a) Mechanical activation time dependence of the average crystallite size of NKN nanocrystalline powder. (b) Size distribution of NKN particle triggered for 2 h. (c) Size distribution of NKN particle triggered for 20 h. (d) and (e) TEM micrographs of the powders subjected to 2 h and 20 h of mechanical activation, respectively.

It is well known that planar surfaces of a grain become smoothly curved at high temperatures, which called surface roughening [24,25]. Theoretical analyses and the influence of surface vacancy concentration on surface roughening [26] show that a few mole percent of surface vacancies can induce surface roughening. Therefore, the interface roughening of oxides can be induced by introducing vacancies through dopant addition.

Comparing the grain boundary (Fig. 5) and the grain morphology (Fig. 6) of NKN ceramics, the grain growth behavior and the interface shape of the grain have a strong correlation. The bigger grain with faceted singular interfaces occurs in the sample for milling 2 h. In contrast, a normal grain growth with smoothly curved rough interfaces occurs in the sample for milling 20 h.

Table 1Cell parameter, cell volume, c/a ratio of NKN milled for different times and relative density of NKN ceramics.

| Sample/cell parameter | a (Å) | b (Å) | c (Å) | Volume | c/a | Relative density |
|-----------------------|-----------|-----------|-----------|----------|--------|------------------|
| Milling 2 h | 3.9431(3) | 5.6739(1) | 5.6414(7) | 126.2143 | 1.4307 | 89.6% |
| Milling 8 h | 3.9441(6) | 5.6705(2) | 5.6395(4) | 126.1256 | 1.4299 | 92.5% |
| Milling 20 h | 3.9452(8) | 5.6659(8) | 5.6359(2) | 125.9824 | 1.4285 | 94.8% |

**Fig. 5.** SEM micrographs of the sintered NKN derived from the powders that were mechanically activated for (a) 2 h, (b) 8 h, and (c) 20 h and then sintered at 1070 °C for 2 h.**Fig. 6.** Grain morphologies of the sintered NKN derived from the powders that were mechanically activated for (a) 2 h and (b) 20 h and then sintered at 1070 °C for 2 h.

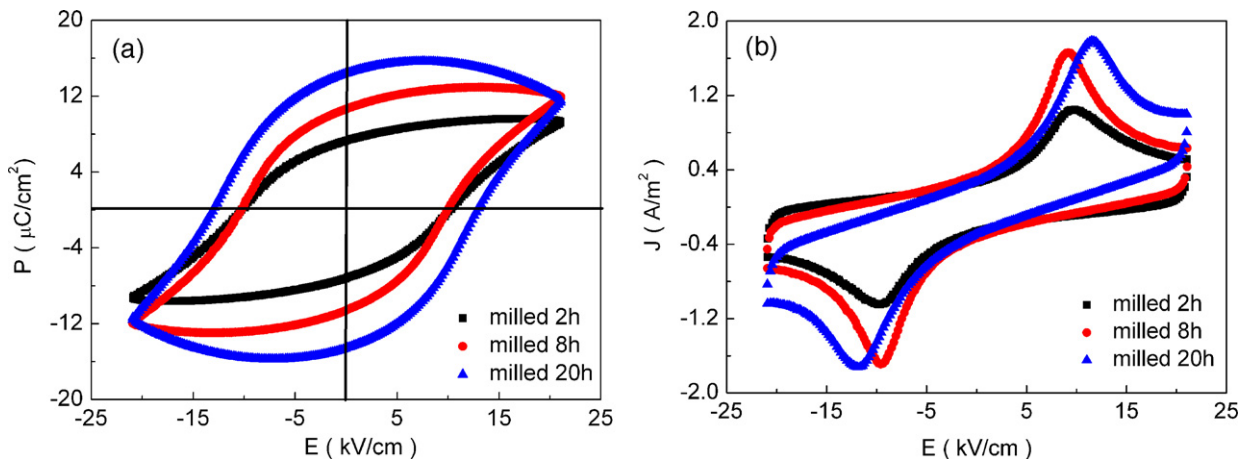


Fig. 7. (a) Ferroelectric hysteresis loops for the NKN milled different times; (b) ferroelectric current density for the NKN milled different times.

The grain size of the sample for milling 20 h is much smaller than that of the sample for milling 2 h (Fig. 5). The slower growth of the grain with a rough interface is most likely due to diffusion-controlled Ostwald ripening [21]. When the growth of the grain is controlled by the diffusion of atoms through a matrix, a stationary and narrow grain size distribution will appear even though the initial distribution is wide. The grain growth with a faceted interface appears to be faster than the grain growth with a rough interface. As a result, the grain size of the sample for milling 20 h is even and fine.

Fig. 7a shows the P - E hysteresis loops of the NKN ceramics milled different times. With the increase in milling time, P_r increases slightly from $7.3 \mu\text{C}/\text{cm}^2$ to $10.6 \mu\text{C}/\text{cm}^2$ and to $14.5 \mu\text{C}/\text{cm}^2$ corresponding to milled 2 h, 8 h and 20 h, while E_c remains 10 kV/mm for milled 2 h and 8 h, but increases to 13 kV/mm. Round-shaped P - E hysteresis loops were obtained in the sample milled 20 h with a higher content of tungsten because of the existence of leakage current (seen in Fig. 7b). It is suggested that the prolonged milling is not favorable to the ferroelectric properties of NKN. Therefore, the NKN milled 8 h shows good ferroelectric properties. The piezoelectric coefficients (d_{33}) of NKN milled 2 h, 8 h and 20 h are 61 pC/N, 91 pC/N and 83 pC/N, respectively. Therefore, NKN milled 8 h yields superior piezoelectric property than that obtained by conventional processing and reported previously [4].

4. Conclusions

$(\text{Na}_{0.5}\text{K}_{0.5})\text{NbO}_3$ nanocrystalline powder and ceramics with different mechanical activation times were fabricated. Mechanical activation led to an improvement in the reactivity of starting materials and therefore the desired NKN phase is formed at a lowered calcination temperature. As the mechanical activation time increases, XRD showed that the orthorhombic distortion of NKN unit cell decreased. SEM showed that the microstructural morphologies changed bimodal to uniform, and that the grain became smaller. These changes are caused by an introduction of impurity (such as tungsten) from milling tools into NKN lattice.

The NKN milled 8 h shows a good ferroelectric property and piezoelectric coefficient.

Acknowledgments

This work was supported by the Natural Science Foundation of China (Grant Nos. 51002036 and 50962004) and the Natural Science Foundation of Guangxi Province (Grant Nos. C013002, 0832003Z, and 0832001).

References

- [1] Z.S. Ahn, W.A. Schulze, *J. Am. Ceram. Soc.* 70 (1987) C18–21.
- [2] Y. Li, J. Wang, R. Liao, D. Huang, X. Jiang, *J. Alloys Compd.* 496 (2010) 282–286.
- [3] L. Egerton, D.M. Dillon, *J. Am. Ceram. Soc.* 42 (9) (1959) 438–442.
- [4] R.E. Jeager, L. Egerton, *J. Am. Ceram. Soc.* 45 (5) (1962) 209–213.
- [5] G.H. Haertling, *J. Am. Ceram. Soc.* 50 (6) (1967) 329–330.
- [6] M. Yang, S. Chu, C. Tsai, *J. Alloys Compd.* 507 (2010) 433–438.
- [7] L. Li, J. Deng, J. Chen, R. Yu, L. Qiao, X. Xing, *J. Alloys Compd.* 471 (2009) 428–431.
- [8] J.S. Benjamin, *Sci. Am.* 234 (5) (1976) 40–48.
- [9] K. Hamada, M. Senna, *J. Mater. Sci.* 31 (7) (1996) 1725–1728.
- [10] L.L. Shaw, Z. Yang, R. Ren, *J. Am. Ceram. Soc.* 81 (3) (1998) 760–764.
- [11] V. Berbenni, A. Marini, G. Bruni, *J. Alloys Compd.* 329 (1–2) (2001) 230–238.
- [12] T. Hungria, J.G. Lisoni, A. Castro, *Chem. Mater.* 14 (4) (2002) 1747–1754.
- [13] V. Berbenni, A. Marini, P. Matteazzi, R. Ricceri, *N.J. Welham, J. Eur. Ceram. Soc.* 23 (3) (2003) 527–536.
- [14] V. Berbenni, A. Marini, *J. Chem. Sci.* 57 (8) (2002) 859.
- [15] T. Rojac, M. Kosec, M. Polomska, B. Hilczer, P. Segedin, A. Bencan, *J. Eur. Ceram. Soc.* 29 (14) (2009) 2999–3006.
- [16] T. Rojac, M. Kosec, B. Malic, J. Holc, *J. Eur. Ceram. Soc.* 26 (16) (2006) 3711–3716.
- [17] V.J. Tennery, K.W. Hang, *J. Appl. Phys.* 39 (1968) 4749–4753.
- [18] M. Ahtee, A.M. Glazer, *Acta Crystallogr. Sect. A: Cryst. Phys. Diffr. Theor. Gen. Crystallogr.* 32 (1976) 434–446.
- [19] O. Perner, J. Eckertl, W. Haßler, C. Fischer, K. HMuller, G. Fuchs, B. Holzappel, L. Schultz, *Sci. Technol.* 17 (10) (2004) 1148–1153.
- [20] Y.M. Chiang, D. Birnie III, W.D. Kingery, *Physical Ceramics: Principles for Ceramic Science and Engineering*, John Wiley & Sons, New York, 1997, pp. 101–184.
- [21] S.Y. Chung, D.Y. Yoon, S.-J.L. Kang, *Acta Mater.* 50 (13) (2002) 3361–3371.
- [22] Y.-I. Jung, S.-Y. Choi, S.-J.L. Kang, *Acta Mater.* 54 (10) (2006) 2849–2855.
- [23] B.K. Lee, S.Y. Chung, S.-J.L. Kang, *Acta Mater.* 48 (7) (2000) 1575–1580.
- [24] F.C. Frank, in: W.D. Robertson, N.A. Gjostein (Eds.), *Metal Surfaces: Structure, Energetics and Kinetics*, American Society for Metals, Metals Park, OH, 1963 p. 1.
- [25] M. Wortis, in: R. Banselow, R.F. Howe (Eds.), *Chemistry and Physics of Solid Surfaces VII*, Springer, Berlin, 1987, p. 367.
- [26] W.K. Burton, N. Cabrera, F.C. Frank, *Philos. Trans. R. Soc. Lond. Ser. A* 243 (1951) 299–358.